BENCHMARK BETWEEN THE PLEIADES/MAIA AND DART FUEL PERFORMANCE CODES ON THE E-FUTURE U-MO/AL DISPERSION FUEL TEST

Denis Lorenzo, Gentien Marois, Hervé Palancher, Stéphane Valance

CEA/DES/IRESNE/DEC, Centre de Cadarache, 13108 Saint Paul lez Durance, France

Bei Ye, Shipeng Shu, Abdellatif Yacout

Argonne National Laboratory, 9700 S Cass Ave, Lemont, IL 60439, USA

ABSTRACT

Argonne and CEA have collaborated to benchmark their respective MTR fuel plate modeling codes (DART and PLEIADES/MAIA) since 2018. Code-to-code comparisons on the most important parameters were performed, such as the evolution of fuel temperature, fuel meat thermal conductivity, swelling, oxide growth, and fuel meat constituent volume fractions. Some of the calculated results were also compared to post-irradiation examination (PIE) data. The benchmark efforts were performed using the data of plate U7MC 4202 irradiated in the E-FUTURE test, which has a fuel meat composition of U-7Mo particles embedded in an Al matrix with 4 wt% Si addition.

The results comparison showed a good overall match between the two codes on all the values of interest and demonstrated a reasonable agreement between calculated and experimental results. Although slight differences were observed, they are understandable. Through this benchmark, the relevance of both DART and PLEIADES/MAIA codes for the simulation of thermo-mechanical behavior of dispersed U-Mo fuel was proved. Furthermore, the observations made throughout this exercise led to identification of parameters adjustments improvement paths for both codes.

1. Introduction

1.1. Context

Dispersed uranium-molybdenum (U-Mo) LEU fuels are investigated as a candidate to replace the HEU fuels used in Material Testing Reactors (MTR). With its utilization as standard MTR fuel, comes the question of predicting its thermo-mechanical behavior in daily operation. Modelling the fuel thermo-mechanical behavior is not only important for the fuel development phase, robust and reliable computing codes are also crucial for preparing its standardized utilization (qualification).

Consolidating knowledge on the behavior of uranium molybdenum fuels necessitates not only the pursuit of irradiation tests but also the capacity to capitalize gained knowledge in predictive simulation codes. In these conditions, Argonne and CEA have decided in 2018 to collaborate in carrying out benchmarks between their respective MTR fuel plate modeling codes DART and MAIA. These codes both associate classical thermo-mechanical computation schemes with specific material evolution laws.

It was decided to start the first series of benchmark on the E-FUTURE irradiation [1] because its data are available in open literature and were obtained at representative operating conditions in a high flux research reactor.

1.2. Previous benchmark effort

The first benchmark exercise [2] between DART and MAIA was initiated on the basis of the E-FUTURE irradiation performed with U-Mo/Al dispersed fuel in the BR2 reactor. The benchmark efforts were performed using the data of plate U7MC 4202, which had a fuel meat composition of U-7Mo particles embedded in an Al matrix with 4 wt% Si addition. On the basis of 2D modelling, the studies aimed at studying the influence of code structure on calculated temperatures, with an approach based on separate-effects tests. Despite differences in the computational approach, the response of the two codes were globally close. The integration of models specific to MTR fuel plates material behavior increased the discrepancies in the fuel core temperature prediction and, as expected, the difference was amplified when models included in a feedback loop with temperature were activated.

1.3. Scope of the current benchmark

1.3.1. General objective

The general objective is to continue and deepen the previous benchmark. In this logic it was decided to work on the same U-Mo/Al fuel plate, namely the U7MC 4202 plate of the E-FUTURE irradiation.

For this benchmark it was chosen to use the 3D version of the MAIA code, in order to access the results on the whole volume of the plate. In this framework it was possible to ensure the loading of heat flux and temperature data on the entire surface of the plate.

1.3.2. Phase-I full code to code comparison

The first phase of this benchmark consists in ensuring a code-to-code comparison of all the computational results, namely: the temperatures of the oxide, the cladding and the fuel meat, the thermal conductivity of the fuel meat, the thickness of the oxide layer, the thickness of the interaction layer and the volume fractions of all the components of the fuel meat (fuel particles, matrix, interaction layer and pores).

It was also decided to carry out parametric studies in order to evaluate the differences in the response of the codes to several key parameters, namely: the concentration of silicon in the matrix (to evaluate the impact on the growth kinetics of the interaction layer), the thermal conductivity of the interaction layer (to evaluate the impact on the thermal conductivity of the fuel meat), the pH (to evaluate the impact on the growth kinetics of the oxide layer) and finally the oxidation model. It should be noted that all these parameters have an impact on the temperature of the fuel meat.

1.3.3. Phase-II comparison with experimental measurements

The objective of the second phase of this benchmark is to compare the results of the two codes to the experimental values measured by SCK CEN on this plate, both for non-destructive [1] and destructive examinations [3]. By comparing the calculation results of the two codes with the real behavior of the fuel under irradiation, this last exercise should allow to consolidate the validation of each code for this type of fuel.

2. Computational codes description

2.1. PLEIADES/MAIA

The MAIA code (Molybdenum uranium Application for Irradiation fuel behavior Analysis) [4], developed by CEA, is a thermo-mechanical simulation code for dispersed fuels (U_3Si_2 and U-Mo) of Material Test Reactors. It is based on the PLEIADES multiphysics and multiscale fuel element simulation platform [5], dedicated to the behavior of nuclear fuels (MAIA for Material Test Reactors, ALCYONE for Pressurised Water Reactors, GERMINAL for Sodium Fast Reactors …). With the tools of the PLEIADES architecture, MAIA offers a user-adaptive computation scheme. The meshes are either bi or tridimensional and cover the main geometries used in MTR reactors, i.e. flat and curved full size plates. The physical models include, among others, the computation of the interaction layer thickness around the fuel particles, a thermal and mechanical homogenization for the fuel meat and several oxidation models for the cladding. A thermal-hydraulic model has recently been integrated. The properties and constitutive laws of the common materials are proposed by default in MAIA. Figure 1 shows several types of geometries and meshes proposed by MAIA.

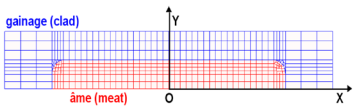

2D mesh of a plane plate

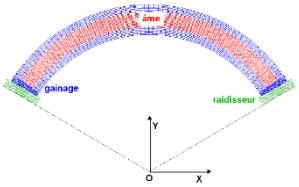

2D mesh of a curved plate with stiffeners

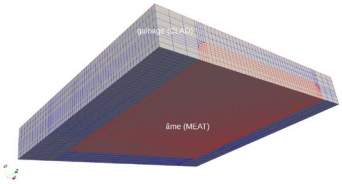

3D mesh of a plane plate

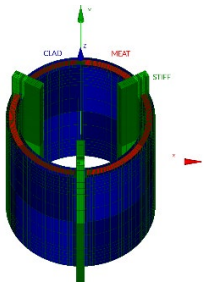

3D mesh of a ring with curved plates

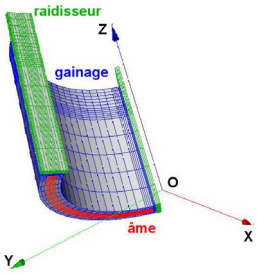

3D mesh of a curved plate with stiffeners

Figure 1 – Illustrations of some design and meshes proposed by MAIA code

2.2. DART

DART (Dispersion Analysis Research Tool) is an integrated fuel performance code developed at Argonne for simulating the irradiation behaviors of research and test reactor fuels [6]. Three calculation branches have been developed for different fuel types: U-Mo/Al dispersion fuel, U-Mo monolithic fuel, and U_3Si_2-Al dispersion fuel. In each calculation branch, assorted thermal, physical, and mechanical models were implemented to simulate the various processes occurring in the fuels during irradiation. The code allows users to define power history, fuel meat configuration, geometry (both miniature-sized and full-sized plates) and meshing of the fuel plates. Besides empirical fuel swelling models, a rate-theory based mechanistic fission

gas swelling model was employed. DART has been validated against measurement results and was used to interpret experimental data in previous studies [7][8]. A three dimensional (3D) heat transfer module and a finite element method (FEM) based mechanical analysis module [9] have been developed and are in the process to be integrated into the code. The code outputs the evolution of fuel meat swelling, microstructure, and temperature, as well as fission gas bubble morphology and local fuel plate deformation due to swelling, etc.

3. Phase I: Full code to code comparison

In this section, the main input parameters and specifications defined for the code-to-code comparison are described. Sensitivity studies were carried out for a number of input parameters and irradiation behavior models. The cases designed for the sensitivity studies and the comparison results are discussed here.

3.1. Input parameters and specifications

Two-dimensional power distributions during the irradiation of plate U7MC 4202, provided by SCK CEN, were applied in the simulations. Selected input parameters and specifications used in both Phase I and II comparisons are listed in Table 1. While most of the parameters and models employed in DART and MAIA are the same, different models for estimating fuel swelling and fuel meat thermal conductivity during irradiation were utilized in the two codes. The impacts of these models on the results are shown in section 3.3. Besides the input parameters indicated in Table 1, the plate and fuel meat dimensions and configurations applied in this study were consistent with the values in [1]. The coolant temperatures were generated using DART with the provided coolant conditions and were applied in both DART and MAIA calculations.

Table 1. Main input parameters and models used in the benchmark study of E-FUTURE plate U7MC 4202.

	MAIA-3D	**DART**
IL composition	*$(U,Mo)Al_4$	
Initial fuel particles volume fraction	48%	
Fuel swelling due to fission products swelling and gaseous swelling	**correlation in Ref. [10]	**correlation in Ref. [11]
Effective fuel meat thermal conductivity (as a function of irradiation)	Method presented in Ref. [4]	Bruggeman model in Ref. [12]
Hydraulic diameter	12 mm	
Fluid velocity	10 m/s	
External pressure	1.2 MPa (nominal BR2 coolant pressure)	
Parameters analyzed	Temperatures, IL thickness, oxide thickness, volume fractions, swelling	

* This composition was chosen as the density of UAl_4 is available. Parametric study were performed for the IL composition of $(U,Mo)Al_3$ – $(U,Mo)Al_6$. Its impact on meat constituent volume fractions is small, and some effect on meat swelling was observed.

** The analytic comparison shows these two correlations give relatively similar results ($\leq$ 5% in difference).

Figure 2 (a) illustrates the schematic of the simulated fuel plate. Although the calculations were performed for the entire fuel meat zone, the comparisons were carried out at selected locations to avoid the uncertainties related to different meshing schemes applied in the two codes. Three axial locations were selected for the results comparison (Figure 2 (b)), representing the maximum, intermediate, and minimum fission density regions, respectively. Code-to-code comparisons were performed at the mid-point of the fuel meat centerline at the selected three axial locations, shown as point A in Figure 2 (c).

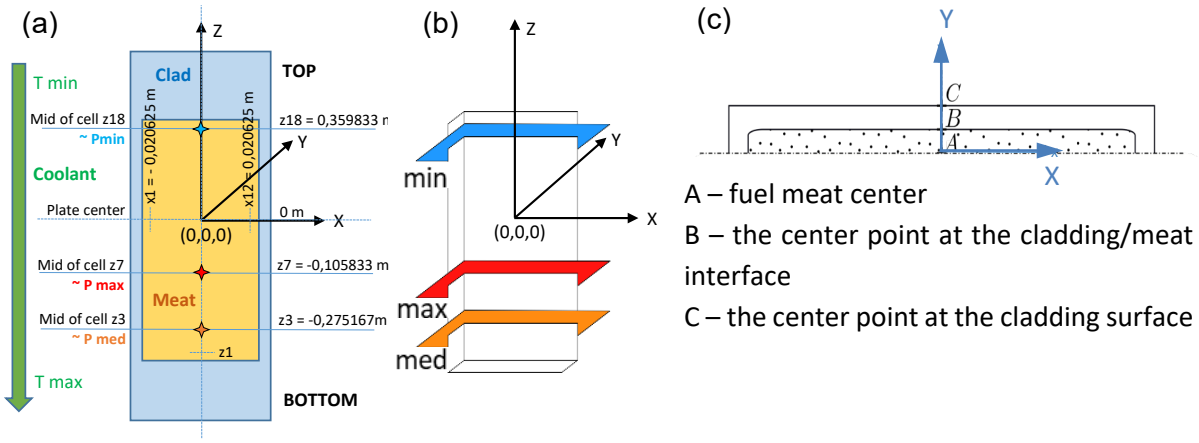

Figure 2. (a) schematic of E-FUTURE plate 4202, (b) the three axial locations (z) selected for comparisons, representing the minimum, intermediate (medium), and maximum fission densities respectively, and (c) planar half cross section of the fuel plate, symmetric on the fuel meat center plane. At each selected axial location, results are compared at point A in (c).

3.2. Studied cases

During the determination of the benchmark specifications, it was identified that several input parameters and models may have stronger influence on fuel meat temperature or swelling behavior than the rest of parameters. Therefore, five study cases were designed for the sensitivity studies of these parameters and models, as listed in Table 2.

Table 2. The parameter/model combinations of the five cases designed for sensitivity studies.

Case ID	Benchmark phase	% Si	IL conductivity	Coolant pH	Oxidation model	U-Mo swelling correlation	
						CEA	ANL
1	U-Mo Phase-I	0%	5 W/(m.K)	6.0	Model 1 [13]	[10]	[11]
2		0%	10 W/(m.K)	6.0			
3		4%	5 W/(m.K)	6.2			
4		4%	5 W/(m.K)	6.0			
5	U-Mo Phase-II	4%	5 W/(m.K)	6.2	Model 2 [14]		

3.3. Results and discussions

The calculated quantities of temperatures at various locations, interaction layer (IL) thickness, coolant-side oxide layer thickness, fuel meat constituent volume fractions, and swelling are compared in this section, grouped according to the interested parameters/models selected for parametric study.

The first model examined is the oxide growth model. Model 2 [14] was updated based on Model 1 [13] to improve its agreement with the measured data for high temperature cases. The oxide layer thickness and fuel meat centerline temperature at the axial location of "max fission density" (see Figure 2) calculated using different oxide models and codes are compared in Figure 3. The results show that both codes generated similar results, particularly when Model 2 was applied. Model 2 predicts lower oxide growth than Model 1 (Figure 3 (a)), which leads to lower fuel meat temperature (Figure 3 (b)). It is worth noting that the highest fuel meat temperature during irradiation occurred at the beginning of the third cycle (Figure 3 (b)), instead of the beginning of the irradiation when the heat flux was the highest. This is because the fuel meat thermal conductivity reduced due to the formation of IL and the consumption of the Al matrix in the fuel meat during irradiation (as shown in Figure 4).

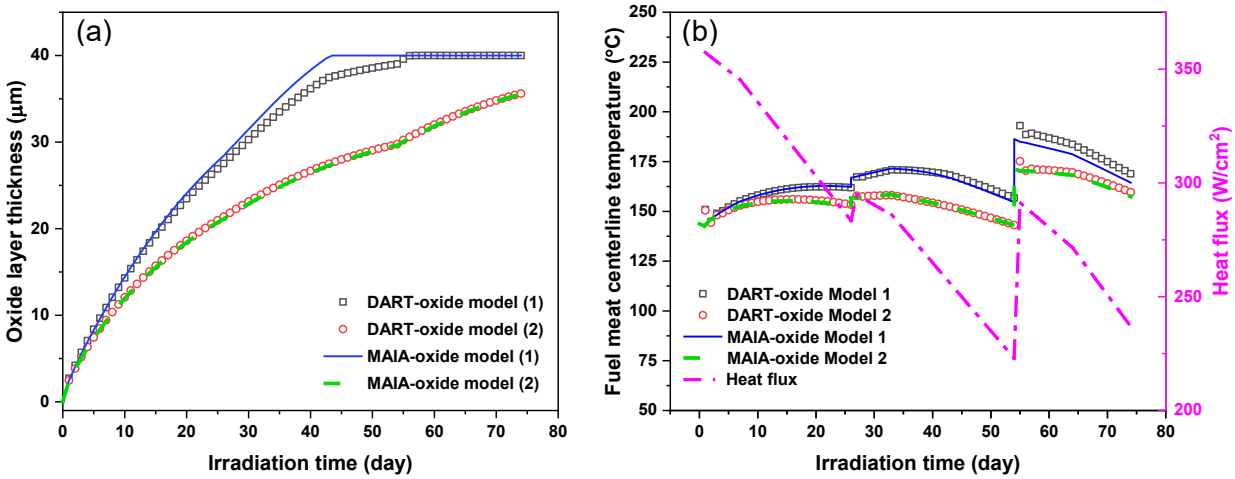

Figure 3. Comparisons of the (a) oxide layer thicknesses and (b) fuel meat centerline temperatures at the axial location of "max fission density" calculated with DART and MAIA, respectively, for cases 3 and 5 in Table 2.

The impacts of the IL thermal conductivity on simulation results can be seen from the comparisons in Figure 4. The IL thermal conductivity is used in estimating effective fuel meat thermal conductivity. The value of 10 W/(m·K) was applied in the previous benchmark in 2019 [2], which was approximated based on literature data. Since then, a direct measurement of the amorphous U-Mo/Al IL thermal conductivity was performed and a value of ~ 5 W/m·K at the operating temperatures of research and test reactors was obtained [15]. Here, these two values were utilized for parametric study. The results show that lower IL thermal conductivity gives lower fuel meat thermal conductivity (Figure 4 (a)) and, consequently, higher fuel meat centerline temperature (Figure 4 (b)). However, it almost has no influence on fuel meat swelling (Figure 4 (c)). Some differences in results can be noticed between the two codes. Particularly when IL thermal conductivity is set to 5 W/m·K, the curves of fuel meat thermal conductivity and centerline temperature predicted by different codes deviate from each other, due to the difference in the models used to calculate fuel meat thermal conductivity. Fuel

swelling results stay unchanged for the same code but are different between the two codes. The difference in fuel swelling presented in Figure 4 (c) is consistent with the difference in the fuel swelling models employed in the two codes. Therefore, such differences are deemed reasonable.

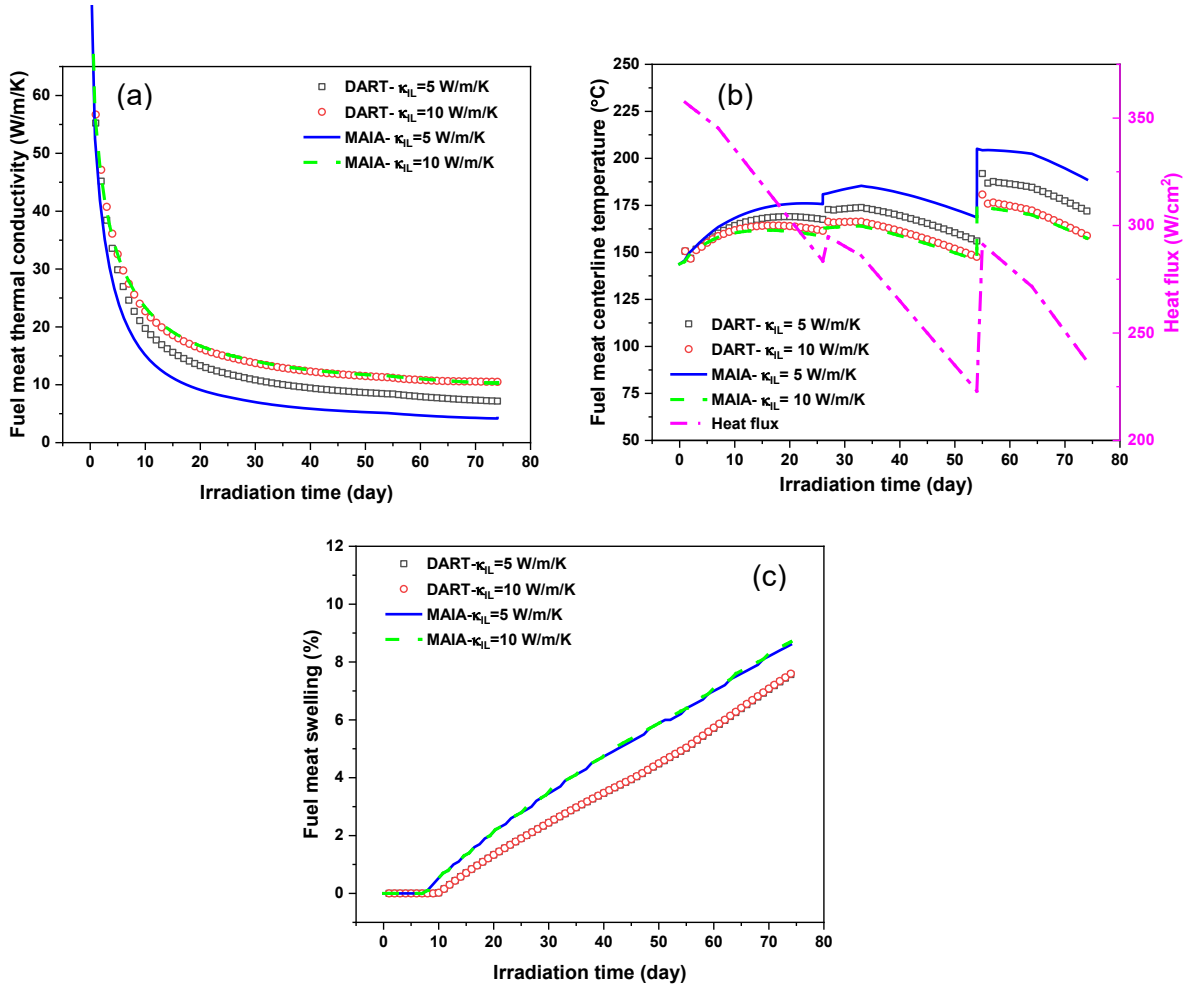

Figure 4. Comparisons of the (a) fuel meat thermal conductivity, (b) fuel meat centerline temperatures, and (c) fuel meat swelling at the axial location of “max fission density” calculated with DART and MAIA, respectively, for cases 1 and 2 in Table 2.

The effect of Si content in the matrix was investigated by comparing the calculation results from cases 1 and 4 in Table 2. As shown in Figure 5, higher Si content led to less IL growth, which in turn resulted in higher fuel meat thermal conductivity. On the other hand, because IL growth is a function of fuel meat temperature, which is governed by fuel meat thermal conductivity, a negative feedback loop exists between the Si content and fuel meat thermal conductivity. Therefore, the divergences between the results of the two Si contents were growing with irradiation time. The results from both codes generally agree with each other. The slight difference is related to the different fuel meat thermal conductivity models employed in the codes. For instance, when Si content is 4 wt%, the codes predicted nearly identical IL thickness (Figure 5 (a)), suggesting very close fuel meat composition was calculated by the two codes. Thus, the discrepancy between the fuel meat thermal conductivity curves of the 4% Si content in Figure 5 (b) demonstrates the effect of the different fuel meat thermal conductivity models used in the codes.

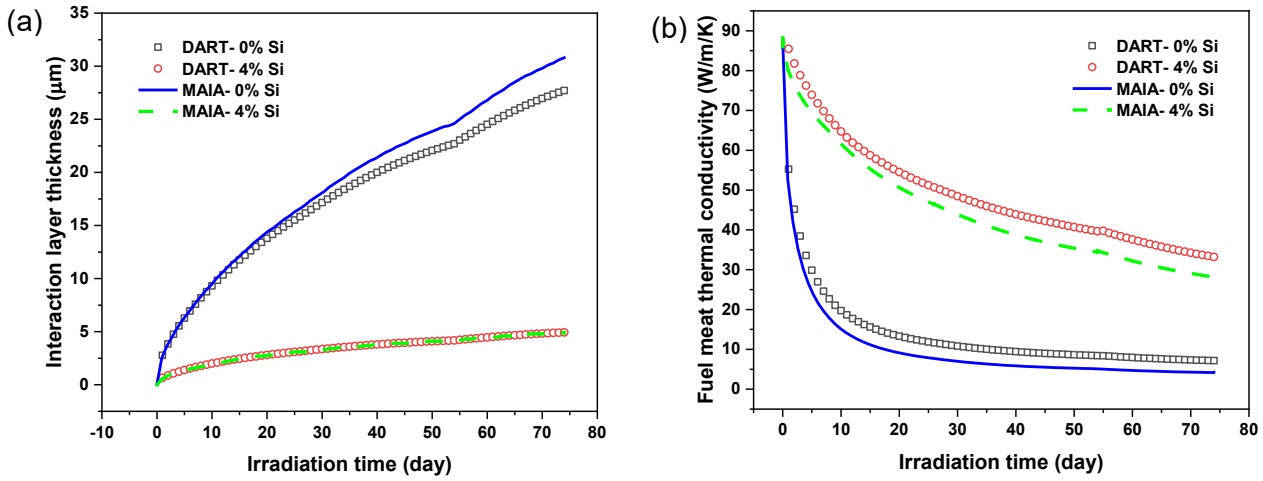

Figure 5. Comparisons of the (a) interaction layer thickness and (b) fuel meat thermal conductivity at the axial location of "max fission density" calculated with DART and MAIA, respectively, for cases 1 and 4 in Table 2.

The predicted oxide layer growth is sensitive to the pH value of the coolant, shown in Figure 6 (a). Varying the pH value from 6.0 to 6.2 almost doubled the oxide layer thickness at the end of irradiation. Consequently, the fuel meat temperature increased ~ 25ºC in the third cycle, as indicated in Figure 6 (b). On the other hand, the differences between the two codes are small, indicating the codes handled the oxide layer growth and the associated processes similarly.

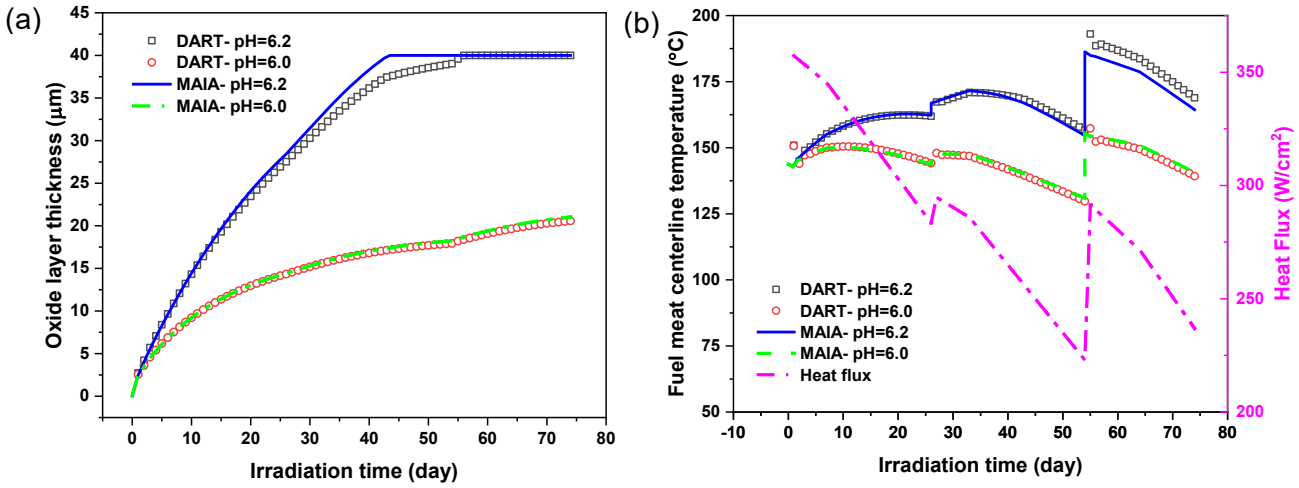

Figure 6. Comparisons of the (a) oxide layer thickness and (b) fuel meat centerline temperature at the axial location of "max fission density" calculated with DART and MAIA, respectively, for cases 3 and 4 in Table 2.

In Figure 7, the calculation results at the three selected axial locations were compared to reveal the effects of fission density. The calculated fuel meat temperature, IL growth, and fuel particle swelling increase with the fission density. Among these parameters, fuel particle swelling is proportional to fission density, while fuel meat temperature and IL growth are primarily associated with fission rate. Since fission density is linearly correlated to fission rate within a single plate, the impact of fission rate on fuel meat temperature and IL growth appears to be related to fission density here. Both codes behave very similarly in predicting fuel meat temperature and IL thickness. Noticeable differences are seen in fuel particle swelling

comparison, caused by the different U-Mo swelling correlations employed as indicated in Table 2.

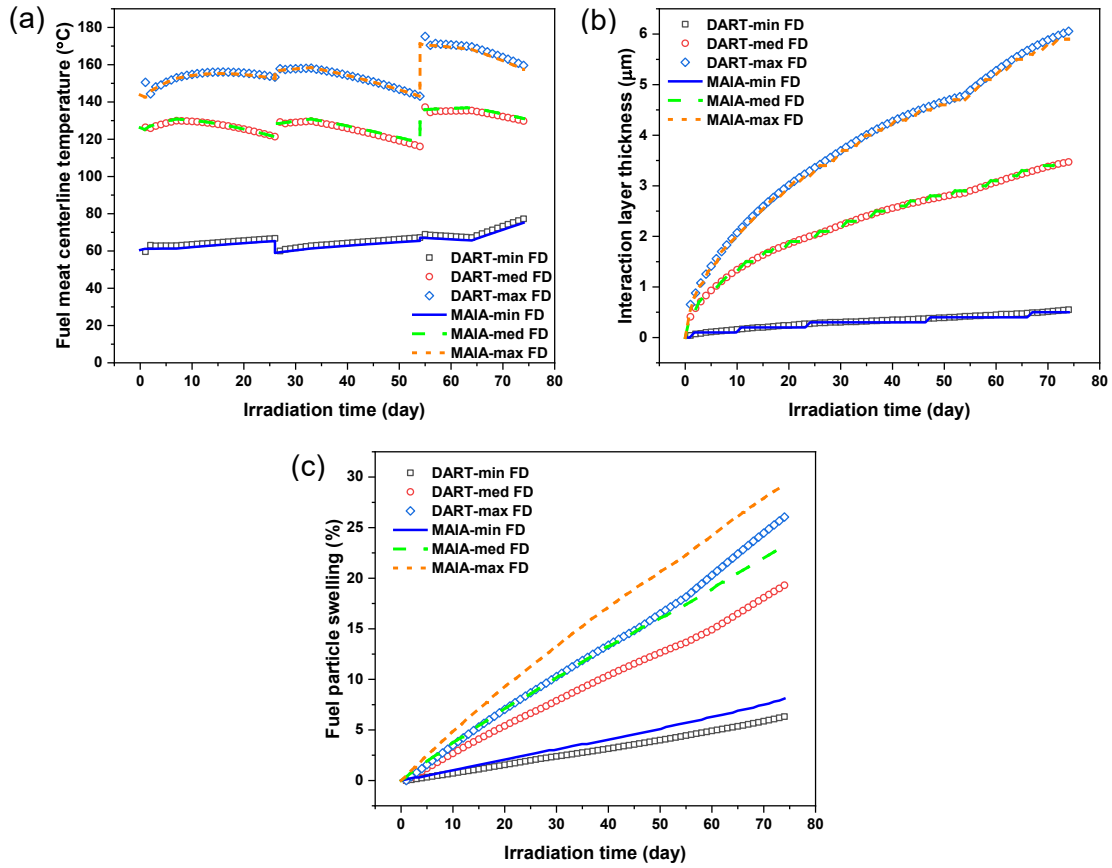

Figure 7. Comparisons of the (a) fuel meat centerline temperature, (b) interaction layer thickness, and (c) fuel particle swelling at the axial locations with different fission densities calculated with DART and MAIA, respectively, for case 5 in Table 2.

4. Phase II comparison with experimental measurements

4.1. Preliminary remark about the construction of the graphs in this chapter

The SCK CEN measurement values were recovered using digitizing tools thanks to the graphs of the non-destructives and destructives examination articles (respectively [1] and [3]).

The light grey circles correspond to the results of MAIA calculations, the dark grey crosses to the results of DART calculations and the blue or red crosses to the destructive and non-destructive examinations carried out by SCK CEN.

4.2. Volume fractions

Figure 8 below shows the evolution of the volume fractions of the fuel meat components as a function of the fission density.

The codes results show reasonable agreement with the experimental measurement values, both in terms of absolute values and trends as a function of fission density.

A significant dispersion of the experimental measurement values can be noted for very small differences in fission density. These discrepancies could be linked at first order to the

measurement uncertainties and perhaps to the heterogeneity of the fuel distribution in the meat, and at second order to temperature differences (the codes do not produce such discrepancies for the calculated temperature differences between these different measurement points).

It should be noted that, unlike the MAIA calculations, DART do not integrate heat edge conduction in the current thermal model, which leads to temperature differences on the axial and lateral plate edges at equivalent fission density. On the three graphs of Figure 8, a filter was applied to MAIA and DART results to remove the axial and lateral edge values and thus allow comparisons between the two codes in the current part.

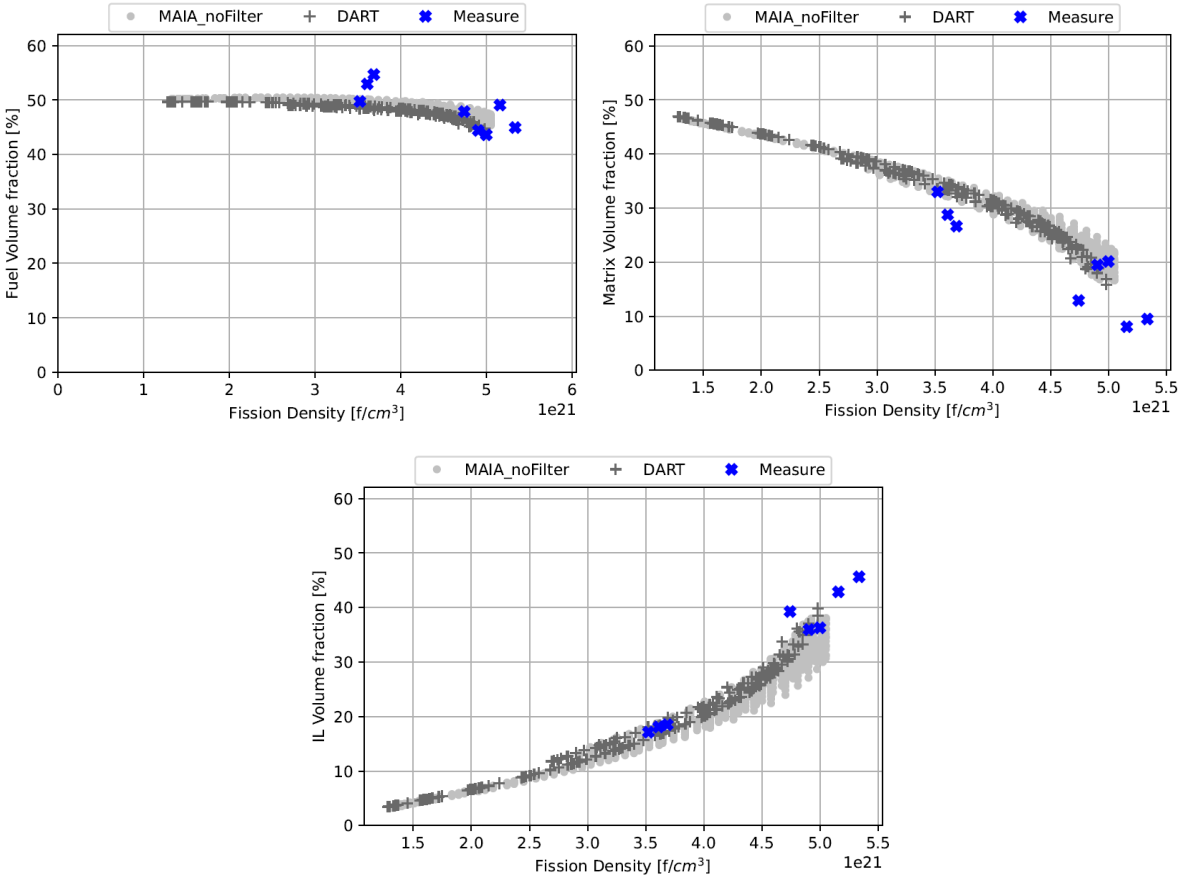

Figure 8. Evolution of the volume fractions of the fuel meat components (fuel, matrix and interaction layer) as a function of the fission density

4.3. Swelling

Figure 9 below shows the evolution of the meat swelling and of the fuel particle swelling as a function of the fission density.

For the fuel particle swelling, as for volume fractions, the codes results show reasonable agreement with the experimental measurement values, both in terms of absolute values and trends as a function of fission density. The difference between the DART and MAIA results is related to the different swelling models used, as explained in paragraph 3.3.

For the meat swelling, one can see a clear difference in slope between calculations and measurement. The main hypothesis on this difference in slope is the conversion between fuel particle swelling and meat swelling:

- the points associated with the experimental measurements are calculated from the values of the deformation measurements of the plates (non-destructive tests) and the volume fraction of the particles in the fresh fuel;
- the results of the calculation codes are obtained from methods of homogenization of the volumes of each component at each time step (fuel + matrix + interaction layer + pores closure).

It can be noted that the extrapolations of the meat swelling curves of the DART and MAIA codes do not pass through the point of origin (0,0): this is related to the assumption of pore closure at the beginning of life.

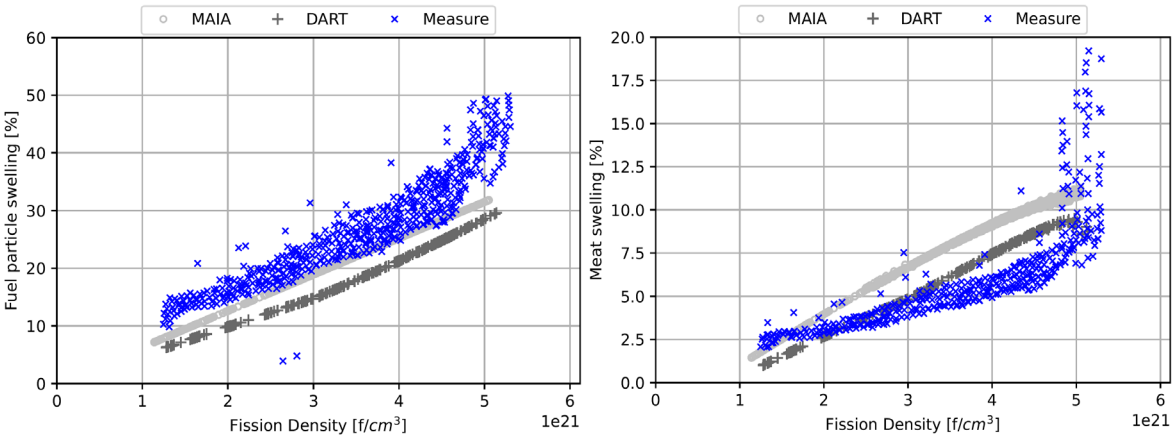

Figure 9. Evolution of the fuel particle swelling (on the left) and of the meat swelling (on the right) as a function of the fission density

4.4. Oxide thickness

The Figure 10 shows the axial profiles of the oxide thickness measured by SCK CEN along 10 equidistant lines between the edges of the fuel meat, on the lower face (left figure) and on the upper face (right figure) of the plate. The 6 mm line corresponds to one lateral edge of the combustible meat and the 51 mm line to the other lateral edge (the width of the combustible meat being 45 mm).

The Figure 11 shows the axial profiles of the oxide thickness, with SCK CEN measurements, DART results and MAIA results:

- SCK CEN measurements along the lines 41 and 46;
- DART results along the line 31 (central axe);
- MAIA results along the lines 31 and between the lines 41 and 46 (left figure) and on the whole surface (right figure).

It is advisable to make some preliminary comments on these curves before analyzing the results:

- the coordinate systems differ between the graphs of Figure 10 and Figure 11 (inversion of the axis and shift of the coordinates), the system used for the calculations having been judged more convenient to use than the one used for the exams (coordinate Z=0 in the middle of the plate and coordinates increasing from the bottom to the top of the plate in reactor);

- the axial profiles between the line 41 and 46 are globally those with the highest peak in the oxide layer thickness. We chose to present those axial profiles because it is precisely on the basis of the highest axial profiles of the E-FUTURE and SELENIUM irradiations that the oxide growth correlation used in MAIA and DART was calibrated [14] (on plates 4202, 4111 and 6301 for the E-FUTURE irradiation, each time along line 41).
- the strong discontinuities in the middle of the measurements curves correspond to the pillowing region, where the oxide appeared to have spalled off (the extensive swelling in the pillowed zone creating high local stresses in the oxide layer). They should therefore not be considered for comparison with the computational results.

The analyses that can be made on the comparison of the calculation curves and the experimental curves of Figure 11 are the following:

- we find the very good correspondence between the DART and MAIA calculation results presented in chapter 3.3. (comparison made along the central axis of the plate);
- compared to the experimental results, the calculated thicknesses of the oxide layer along the lines that cross the area of maximum oxide growth (approximately between lines 41 and 46) are very slightly less (a few microns) at the peak, roughly equal at the ends of the plate (where temperatures are too low to induce significant oxidation) and about ten microns lower in the intermediate areas. The calculated axial profiles are therefore hollower than the experimental axial profiles;
- at the edges of the combustible meat, the MAIA calculations result in very flat profiles: a much more attenuated peak on the side of the maximum oxidation thickness (lines 41 to 46) and a profile close to zero along the entire length of the plate on the opposite side of the maximum oxidation thickness (lower grey points in the right-hand figure in Figure 5). With the used oxidation correlation, this much lower oxidation level is related to the overcooling of the combustible meat at the edges of the plate (lateral heat conduction). The strong thermal gradient of the oxide layer on the lateral sides of the plate can be visualized on the 2D mapping presented in Figure 12. It can be noticed that the measurements performed on the plate edges also show a very attenuated peak and a profile close to zero, although they are inverted compared to the calculation results. It is therefore possible that these lower experimental values actually does not reflect only an edge effect on eddy current as hypothesized in [1], but also a real lower level of oxidation at the edges of the plate due to the drop in temperature.

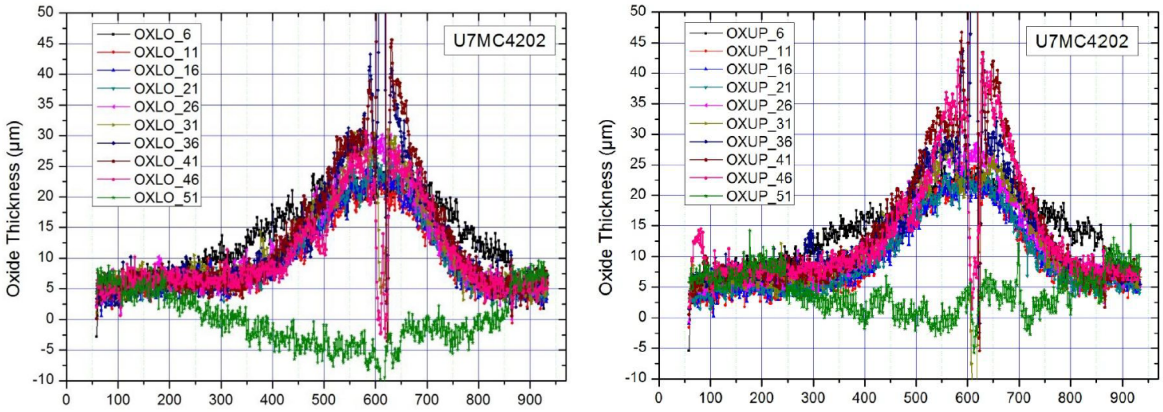

Figure 10. Oxide thickness profile along the length of the plate – SCK CEN measurements as a function of the distance to the plate edge on the lower side (left figure) and on the upper side (right figure) of the plate

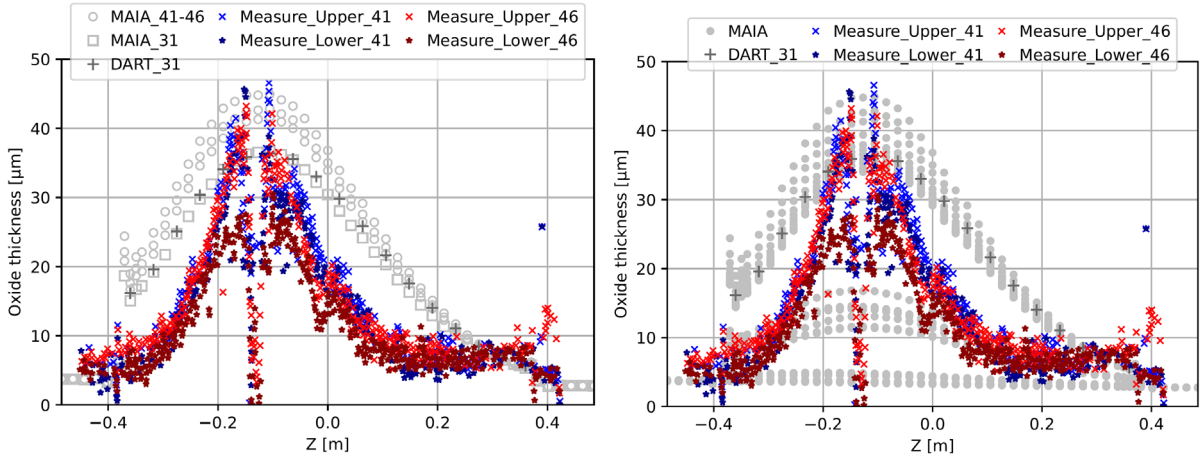

Figure 11. Oxide thickness profile along the length of the plate - SCK CEN measurements along the lines 41 and 46 / DART results along the line 31 (central axe) / MAIA results along the line 31 and between the lines 41 and 46 (left figure) and on the whole surface (right figure)

Figure 13 shows a 2D mapping of the oxide thickness over the plate area for the DART calculations, MAIA calculations and SCK CEN measurements. The value scales have been harmonized between these different results so that they are visually comparable. The DART and SCK CEN maps are given only on the cladding surface facing the fuel meat, while the MAIA map is given on the whole surface of the plate, with the frame and the aluminum cladding extending laterally from the zone located above the fuel meat. The edge effects mentioned above for the MAIA calculations are easily identifiable: they are the gray lines located at the edge of the fuel meat, along the aluminum frame in blue (oxidation level close to zero). Measurement edge effects, whether related to measurement artifacts or lateral heat conduction (or a combination of both), are also clearly identifiable on the SCK CEN map. Otherwise, we find the very good correspondence of results between MAIA and DART calculations, and the hollower character of the oxidation peak for SCK CEN measurements compared to the DART and MAIA calculations, whose significant oxidation zone spreads more widely around the peak.

On the whole, the calculation results for the oxide thickness are therefore in correct agreement with the measurements.

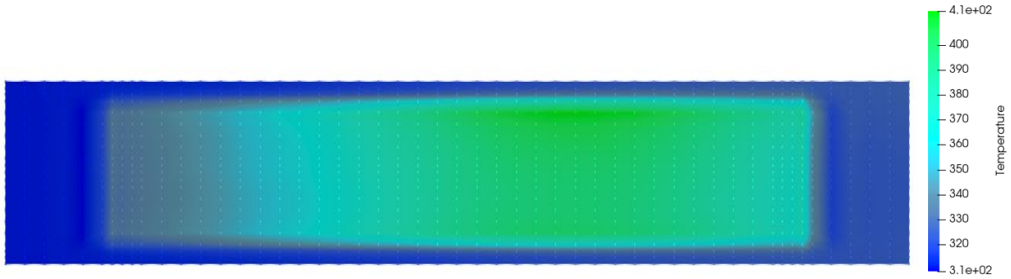

Figure 12. 2D map of the oxide layer temperatures calculated (MAIA) at the beginning of the first cycle (temperatures in degrees Kelvin)

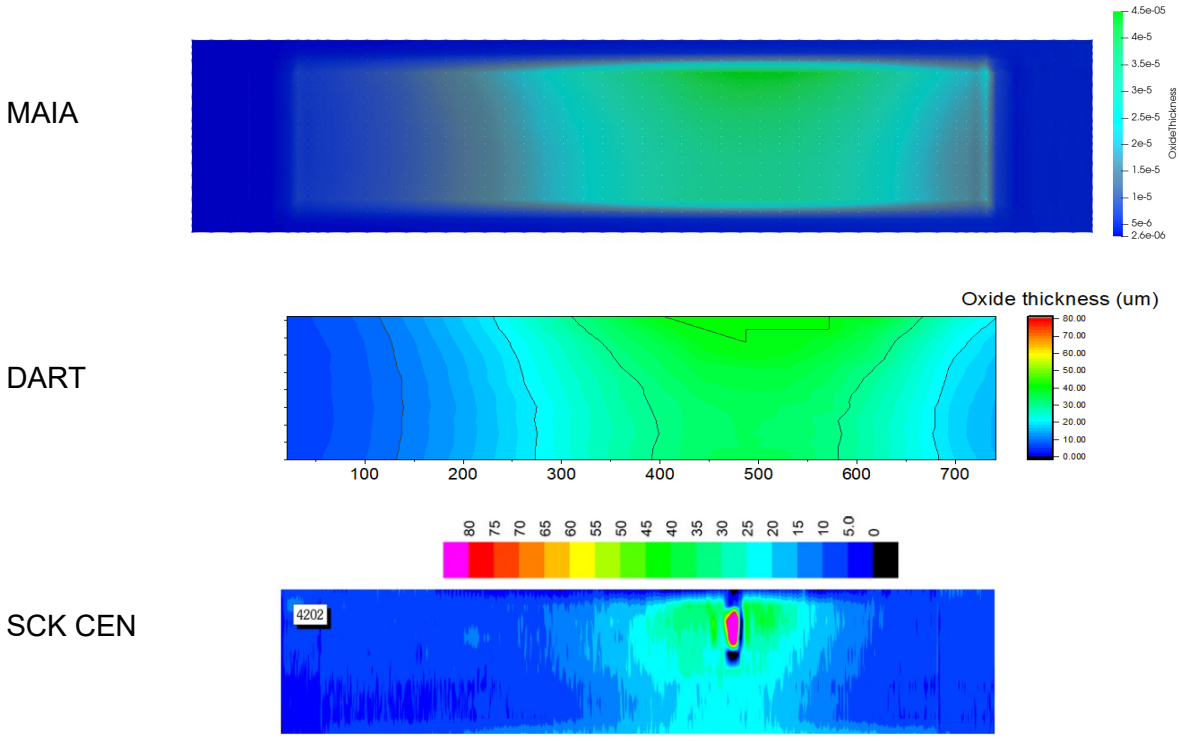

Figure 13. From top to bottom: 2D maps of oxide thicknesses for MAIA calculation results on the whole plate (in meters), for DART calculation results above the fuel meat (in microns) and for SCK CEN measurements of the upper side of the plate above the fuel meat (in microns)

5. Summary and future work

The agreement between the codes is reasonable. In many cases, the results are almost identical. Small discrepancies are observed for fuel meat/fuel particle swelling and fuel meat thermal conductivity comparisons, which are due to different models. The parametric study shows that fuel meat temperature is sensitive to oxide growth model, IL thermal conductivity, pH value, and Si content in the matrix. Fuel meat temperature reached the peak value at the beginning of the third cycle, despite a lower heat flux compared to the BOL, because of the degradation of fuel meat thermal conductivity.

The agreement between the calculated and measured results is reasonable for all parameters considered, and assumptions are made about the few differences found.

Future work includes the benchmarks on coated U-Mo/Al dispersion fuel and silicide fuel (irradiations to be defined).

Acknowledgements

BY, SS, and AY fully acknowledges the support of the U.S. Department of Energy, National Nuclear Security Administration (NNSA), Office of Material Management and Minimization (NA-23) Reactor Conversion Program under Contract No. DE-AC02-06CH11357. Argonne, a U.S. Department of Energy Office of Science laboratory, is operated under Contract No. DE-AC02-06CH11357. The U.S. Government retains for itself, and others acting on its behalf, a paid-up nonexclusive, irrevocable worldwide license in said article to reproduce, prepare derivative works, distribute copies to the public, and perform publicly and display publicly, by or on behalf of the Government.

References

[1] S. Van den Berghe, Y. Parthoens, F. Charollais, Y. Kim, A. Leenaers, E. Koonen, V. Kuzminov, P. Lemoine, C. Jarousse, H. Guyon, D. Wachs, D. Keiser, A. Robinson, J. Stevens and G. Hofman, Swelling of U(MO)-Al(Si) dispersion fuel under irradiation - Non-destructive analyses of the LEONIDAS E-FUTURE plates, Journal of Nuclear Materials: 430(1-3), 2012.

[2] S. Valance, A. Monnier, H. Palancher (CEA) B. Ye, A. Yacout (ANL), Benchmarking of the thermal chain of the MTR Fuel simulation codes DART-2D and MAIA, RRFM, 2019.

[3] A. Leenaers, S. V. d. Berghe, J. V. Eyken, E. Koonen, F. Charollais, P. Lemoine, Y. Calzarava, H. Guyon, C. Jarousse, D. Geslin, D. Wachs, D. Keiser, A. Robinson, G. Hofman and Y. Kim, Microstructural evolution of U(Mo)–Al(Si) dispersion fuel under irradiation – Destructive analyses of the LEONIDAS E-FUTURE plates, Journal of Nuclear Materials 441, pp. 439-448, 2013.

[4] V. Marelle, F. Huet and P. Lemoine, Thermo-mechanical modelling of U-Mo fuels with MAIA, Research Reactor Fuel Meeting, 2004.

[5] B. Michel & al. (CEA), Two fuel performance codes of the PLEIADES platform: ALCYONE and GERMINAL, Nuclear Power Plant Design and Analysis Codes, pp. 207-233, 2021.

[6] J. Rest, The DART dispersion analysis research tool: a mechanistic model for predicting fission-product-induced swelling of aluminium dispersion fuels, ANL-95/36, 1995.

[7] B. Ye, G. Hofman, A. Leenaers, V. Bergeron, V. Kuzminov, S. van den Berghe, Y. Kim and H. Wallin, A modelling study of the inter-diffusion layer formation in U-Mo/Al dispersion fuel plates at high power, Journal of Nuclear Materials: 499, 2018.

[8] B. Ye, J. Rest, Y. Kim, G. Hofman and B. Dionne, DART analysis of irradiation behavior of U-Mo/Al dispersion fuels, Nuclear Technology: 191(1), 2015.

[9] S. Shu, Y.S. Kim, B. Ye, A. Oaks, K. Mo, A. Yacout, A. Robinson (ANL), Dispersion fuel mechanical analysis model developement for the DART fuel performance code, in Proceedings of the RRFM 2022 conference, 2022.

[10] V. Marelle, S. Dubois, M. Ripert, J. Noirot, P. Lemoine (CEA), MTR plates modeling with MAIA, in RERTR-2007, Prague, 2007.

[11] Y.S. Kim, G.L. Hofman (ANL), Fission product induced swelling of U-Mo alloy fuel, Journal of Nuclear Materials 419 (2011), pp. 291-301, 2011.

[12] J. Rest, Y.S. Kim, G.L. Holmes (ANL), M.K. Meyer, S.L. Hayes (INL), U-Mo Fuels Handbook Version 1.0, ANL-09/31, 2006.

[13] T. Chae, Y. Kim, A. Yacout, Overview of Aluminium Oxide Prediction Models for High Power Research Reactors, ANL/RTR/TM-18/10, 2018.

[14] Y. Kim, H. Chae, S. Van den Berghe, A. Leenaers, V. Kuzminov and A. Yacout, Aluminium cladding oxide growth prediction for high flux research reactors, Journal of Nuclear Materials 529, 2020.

[15] Y. Miao, et. al., Thermal conductivity measurement of the interaction layer between U-Mo and Al produced by high-energy heavy ion irradiation, Journal of Nuclear Materials 539 (2020) 152262, 2020.